Investigation of electronic transport in carbon nanotubes using Green's-function method

Umegaki, Toshihito
Ogawa, Matsuto
Miyoshi, Tanroku

(Citation)
Journal of Applied Physics,99(3):034307-034307

(Issue Date)
2006-02-01

(Resource Type)
journal article

(Version)
Version of Record

(URL)
https://hdl.handle.net/20.500.14094/90000823

Investigation of electronic transport in carbon nanotubes using Green's-function method

Toshihito Umegaki,[a] Matsuto Ogawa, and Tanroku Miyoshi
Graduate School of Science and Technology, Kobe University, 1-1 Rokkodai, Nada-ward, Kobe City 657-8501 Japan

(Received 27 June 2005; accepted 21 December 2005; published online 8 February 2006)

We have investigated the fundamental transport characteristics in carbon nanotubes (CNTs) in order to realize a high-frequency device. In the present analysis, the electron and hole densities are excited at each lead and propagate as a wave from the left contact to the right contact in the CNTs. First, we applied Green's-function method formulation to CNTs with arbitrary chirality. We then calculated the basic conductive characteristics in the CNTs. In the metallic and intrinsic CNTs, the assumption of a linearly varying potential distribution is valid because the electron and hole densities satisfy the charge neutrality condition, and their distributions become uniform. We evaluated the *I-V* characteristics of semiconductive and metallic CNTs. Based on the obtained results, we can control the differential conductance from a negative value to a value of several times the conductance quantum by means of chirality, Fermi level, and bias voltage. We evaluated the *GV*/*I-V* characteristics of the *zigzag* CNT and found that when the group velocity of a mode with a real wave vector is comparable to that of another mode, *GV*/*I* takes a maximum at V_0, which corresponds to the transition between these modes. © *2006 American Institute of Physics*. [DOI: 10.1063/1.2169877]

I. INTRODUCTION

Recently, several types of analytical methods for quantum transport in carbon nanotubes (CNTs) have been studied. Tamura and Tsukada reported a tight-binding method for conductance calculation of nanotube junctions.[1] Ando *et al.* evaluated the effective-mass theory for CNTs and showed that the conductance is quantized into integer multiples of the conductance quantum $e^2/\pi\hbar$.[2] Anantram showed that the differential conductance of CNTs is related to the bias voltage applied to the CNT and the CNT diameter.[3] Triozon *et al.* showed a method for discriminating defects in a CNT by evaluating the Fermi-level-dependent transport.[4] Latil *et al.* derived the mean free path in CNTs and the conductance by combining first-principles methods to tight-binding approaches and took into account the chemical nature of impurities.[5] We have studied the basic conductive characteristics in CNTs using a transfer-matrix (TM) method.[6] Based on these results, we have previously proposed a ferrite device that acts as a filter in the terahertz frequency domain. In order to evaluate the basic conductive characteristics of CNTs more precisely, we herein report an application of Green's-function method (GFM).

For the one-dimensional case, Green's-function method has been successfully applied to the analysis of quantum devices.[7] Chibotaru *et al.* treated the GFM for CNTs and showed that the self-energy matrix has the dimension of the number of contacted carbon atoms in one lead.[8] Anantram *et al.* discussed the physics of a CNT side contacted to metal by using the GFM.[9] In order to analyze CNTs, each of which is connected to two leads, we will extend the methods applied to the analysis of quantum transport in semiconductors.[10] Since our GFM formulation is applicable to CNTs with arbitrary chirality, even those with carbon atom vacancies, we can evaluate not only metallic CNTs but also semiconductive and insulating CNTs. In addition, since the proposed method can be used to evaluate not only current but also electron and hole densities in CNTs, we can solve Green's function and the Poisson equation simultaneously. This GFM can be extended further to

(1) evaluate alternating current and
(2) evaluate interactions between electronic waves and the electromagnetic field,

in the analysis of quantum transport phenomena in CNTs.

As a first step, in Sec. II, we derive equations of electronic transport in CNTs. Next, in Sec. III, we formulate the retarded Green's function. In Sec. IV, we apply the formula to the analysis of quantum transport in CNTs. In the present study, we focus on

(1) the electron and hole density distributions for a metallic and intrinsic CNT with (6, 0) chirality,
(2) the multimode effect and evanescent electronic waves in a semiconductive CNT with (16, 0) chirality,
(3) transitions between the modes in the (16, 0) CNT and the corresponding experimental data,[11]
(4) comparison of the present findings with the experimental *I-V* characteristics[11] in a CNT with (14, 0) chirality, and
(5) the multimode effect and evanescent electronic waves in a metallic CNT with (18, 18) chirality.

Our conclusions are summarized in the final section of the study.

[a]Also at Department of Electrical and Electronics Engineering, Kobe University, 1-1 Rokkodai, Nada-ward, Kobe City 657-8501, Japan; electronic mail: drplum@blue.livedoor.com

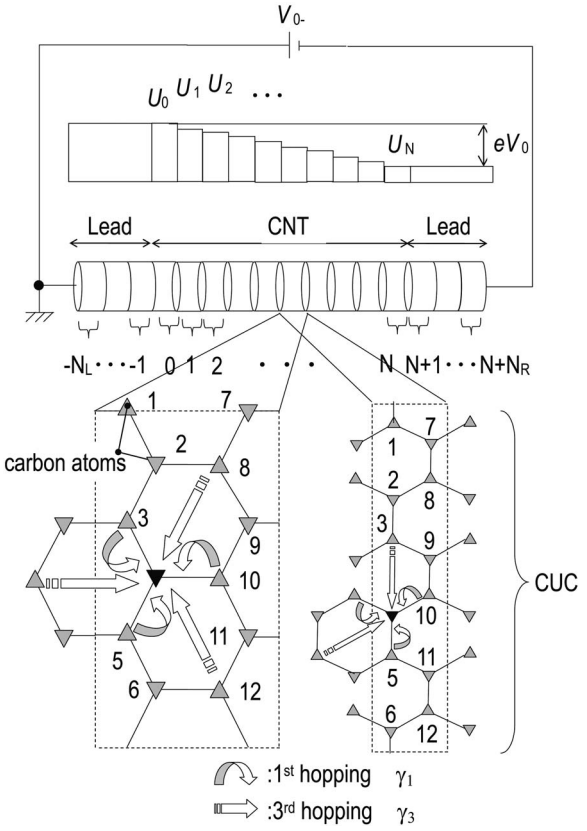

FIG. 1. Schematic models of the CNTs viewed as coaxially rolled graphite sheets under a biased condition. The left and right CUCs correspond to *zigzag* and *armchair* CNTs, respectively.

II. EQUATIONS OF ELECTRONIC TRANSPORT IN CNTs

Starting from the Schrödinger equation for the wave function $|\Psi\rangle$ of an electron in a CNT, which is expressed as

$$\hat{H}|\Psi\rangle = E|\Psi\rangle, \tag{1}$$

Fig. 1 shows a schematic model of a CNT with two leads under an applied bias voltage V_0. The CNT consists of $N+1$ CNT unit cells (CUCs), a lead connected to the left end of a CNT that consists of N_L CUCs, and a lead connected to the right end of a CNT that consists of N_R CUCs. The CUC of each CNT has $4n$ carbon atoms. In particular, an $(n,0)$ nanotube is called a *zigzag* nanotube and an (n,n) nanotube is called an *armchair* nanotube.[6] The left and right enlargements in Fig. 1 correspond to the zigzag and armchair CNTs $(n=3)$, respectively. Blase *et al.* showed that π^*-σ^* hybridization can occur in small nanotubes which change the electronic band structure from that obtained by simply folding the graphite sheet band structure.[12] On the other hand, our formalism assumes a π-orbital approximation, which applies only to tubes with a sufficient radius. The (3, 0) CNT is considered only for illustration of our theory, while this theory actually applies to tubes with a larger radius. In Fig. 1, the wave function $|\Psi\rangle$ is expanded as

$$|\Psi\rangle = \sum_{j=-N_L}^{N+N_R} \sum_{k=1}^{4n} \langle e_{j,k}|\Psi\rangle |e_{j,k}\rangle, \tag{2}$$

with the tight-binding basis,

$$\{|e_{j,k}\rangle, \quad j=-N_L,\ldots,N+N_R, \quad k=1,2,\ldots,4n\}. \tag{3}$$

Now, we consider the on-site energy E_j at the kth carbon atom in jth CUC, and hopping energies γ_1, γ_3, namely,

$$\langle e_{j,k}|\hat{H}|e_{j',k'}\rangle \equiv \begin{cases} E_j & (j,k)=(j',k') \\ \gamma_1 & (j,k) \text{ and } (j',k') \text{ are nearest neighbors} \\ \gamma_3 & (j,k) \text{ and } (j',k') \text{ are the third-nearest neighbors} \\ 0 & \text{otherwise,} \end{cases} \tag{4}$$

where γ_1 is 2.31 eV. We consider the third-nearest neighbors, γ_3, to avoid a matrix singularity, which will be discussed later. The curved arrows that point toward "▼" represent nearest-neighbor interactions, whereas the straight arrows represent the third-nearest-neighbor interactions. Taking the inner products of (1) and (3), we obtain the Schrödinger equation for the zigzag CNT,

$$\begin{bmatrix} H_L & \tau_{LD} & 0 \\ {}^t\tau_{LD} & H_D & \tau_{DR} \\ 0 & {}^t\tau_{DR} & H_R \end{bmatrix} \begin{bmatrix} \psi_L \\ \psi_D \\ \psi_R \end{bmatrix} = E \begin{bmatrix} \psi_L \\ \psi_D \\ \psi_R \end{bmatrix}, \tag{5}$$

where ${}^t\tau_{LD}$ and ${}^t\tau_{DR}$ represent the transposed matrices of τ_{LD} and τ_{DR}, respectively, and the matrices H_L, H_D, H_R, τ_{LD}, and τ_{DR} are defined as

$$H_L = \begin{bmatrix} H_0 & V & & 0 \\ \ddots & \ddots & \ddots & \\ & {}^tV & H_0 & V \\ 0 & & {}^tV & H_0 \end{bmatrix},$$

$$H_D = \begin{bmatrix} H_0 & V & & 0 \\ {}^tV & H_1 & V & \\ & \ddots & \ddots & \ddots \\ 0 & & {}^tV & H_N \end{bmatrix}, \tag{6}$$

$$H_R = \begin{bmatrix} H_N & V & & 0 \\ {}^tV & H_N & V & \\ & \ddots & \ddots & \ddots \\ 0 & & {}^tV & H_N \end{bmatrix},$$

$$\tau_{LD} = \begin{bmatrix} & 0 \\ V & \end{bmatrix}, \quad \tau_{DR} = \begin{bmatrix} & 0 \\ V & \end{bmatrix}, \tag{7}$$

where the matrix τ_{LD} has N_L rows and $(N+1)$ columns, and the matrix τ_{DR} has $(N+1)$ rows and N_R columns. The matrices H_j and V of the zigzag CNT are defined as

$$H_j = \begin{bmatrix} H_{j,1} & V_{\text{int}} \\ V_{\text{int}} & H_{j,1} \end{bmatrix}, \quad V = \begin{bmatrix} 0 & 0 \\ V_{\text{mut}} & 0 \end{bmatrix}. \tag{8}$$

$$H_{j,1} = \begin{bmatrix} E_j & \gamma_1 & & & & \gamma_1 \\ \gamma_1 & E_j & \gamma_1 & & 0 & \\ & \gamma_1 & E_j & \gamma_1 & & \\ & & \gamma_1 & E_j & \gamma_1 & \\ & 0 & & \gamma_1 & E_j & \gamma_1 \\ \gamma_1 & & & & \gamma_1 & E_j \end{bmatrix}, \tag{9a}$$

$$V_{\text{int}} = \begin{bmatrix} 2\gamma_3 & 0 & 0 & 0 & 0 & 0 \\ 0 & \gamma_1 & 0 & 2\gamma_3 & 0 & 2\gamma_3 \\ 0 & 0 & 2\gamma_3 & 0 & 0 & 0 \\ 0 & 2\gamma_3 & 0 & \gamma_1 & 0 & 2\gamma_3 \\ 0 & 0 & 0 & 0 & 2\gamma_3 & 0 \\ 0 & 2\gamma_3 & 0 & 2\gamma_3 & 0 & \gamma_1 \end{bmatrix},$$

$$V_{\text{mut}} = \begin{bmatrix} \gamma_1 & 0 & 2\gamma_3 & 0 & 2\gamma_3 & 0 \\ 0 & 2\gamma_3 & 0 & 0 & 0 & 0 \\ 2\gamma_3 & 0 & \gamma_1 & 0 & 2\gamma_3 & 0 \\ 0 & 0 & 0 & 2\gamma_3 & 0 & 0 \\ 2\gamma_3 & 0 & 2\gamma_3 & 0 & \gamma_1 & 0 \\ 0 & 0 & 0 & 0 & 0 & 2\gamma_3 \end{bmatrix}. \tag{9b}$$

$\boldsymbol{\psi}_L$, $\boldsymbol{\psi}_D$, and $\boldsymbol{\psi}_R$ are the wave functions, which are defined as

$$\boldsymbol{\psi}_L = \begin{bmatrix} \boldsymbol{\psi}_{-N_L} \\ \vdots \\ \boldsymbol{\psi}_{-2} \\ \boldsymbol{\psi}_{-1} \end{bmatrix}, \quad \boldsymbol{\psi}_D = \begin{bmatrix} \boldsymbol{\psi}_0 \\ \boldsymbol{\psi}_1 \\ \vdots \\ \boldsymbol{\psi}_N \end{bmatrix}, \quad \boldsymbol{\psi}_R = \begin{bmatrix} \boldsymbol{\psi}_{N+1} \\ \boldsymbol{\psi}_{N+2} \\ \vdots \\ \boldsymbol{\psi}_{N+N_R} \end{bmatrix}, \tag{10}$$

$$\boldsymbol{\psi}_j = \begin{bmatrix} \psi_{j,1} \\ \psi_{j,2} \\ \psi_{j,3} \\ \psi_{j,4} \\ \psi_{j,5} \\ \psi_{j,6} \\ \psi_{j,7} \\ \psi_{j,8} \\ \psi_{j,9} \\ \psi_{j,10} \\ \psi_{j,11} \\ \psi_{j,12} \end{bmatrix}, \quad \psi_{j,k} = \langle e_{j,k} | \Psi \rangle,$$

$$j = -N_L, -N_L+1, \ldots, N+N_R, \quad k = 1,2,\ldots,12. \tag{11}$$

Similarly, we can easily obtain Schrödinger equations for the armchair or *chiral* CNTs.

Formulations of characteristic equations

The wave function is expanded in the plane wave (PW) basis as

$$\psi_{j,k} = \sum_{i_x=1}^{6} (\kappa_k^{i_x} T_j^{i_x} + \lambda_k^{i_x} R_j^{i_x}),$$
$$j = \ldots, -1, 0, \quad k = 1,2,\ldots,12, \tag{12}$$

at the left lead, where $T_j^{i_x}$ is the amplitude of waves propagating from left to right, and $R_j^{i_x}$ is that of waves propagating in the opposite direction. We define $\kappa_k^{i_x}$ as $\psi_{0,k}$, whose waves propagate from left to right, and $\lambda_k^{i_x}$ is $\psi_{0,k}$, whose waves propagate in the opposite direction, where $k=1, 2,\ldots,12$, $i_x = 1, 2,\ldots,6$, that is, the impinging and outgoing waves at the interface between the left electrode and the CNT. In the left lead, making use of the periodic nature or Bloch's theorem, we can relate the amplitudes of the waves with wave vectors $k_L^{i_x\pm}$ $(i_x = 1,2,\ldots,6)$ as follows:

$$T_{-1}^{i_x} = e^{-ik_L^{i_x+}S} T_0^{i_x}, \tag{13a}$$

$$T_1^{i_x} = e^{+ik_L^{i_x+}S} T_0^{i_x}, \tag{13b}$$

$$R_{-1}^{i_x} = e^{-ik_L^{i_x-}S} R_0^{i_x}, \tag{14a}$$

$$R_1^{i_x} = e^{+ik_L^{i_x-}S} R_0^{i_x}, \tag{14b}$$

where S is the length of a CUC along the CNT. At the left lead, using Eq. (13) and (14) and the following conditions:

$$T_j^{j_x} = \delta_{i_x,j_x}, \tag{15a}$$

$$R_j^{j_x} = 0, \tag{15b}$$

δ_{i_x,j_x}:Kronecker's delta $\quad (j = -1,0,1 \quad j_x = 1,2,\ldots,6)$.

A characteristic equation of the plane wave with wave vectors $k_L^{i_x+}$ can be obtained as follows:

$$\begin{bmatrix} -V_{\text{int}} & EI - H_{0,2} \\ 0 & -V_{\text{mut}} \end{bmatrix}^{-1} \begin{bmatrix} V_{\text{mut}} & 0 \\ H_{0,1} - EI & V_{\text{int}} \end{bmatrix} \begin{bmatrix} \boldsymbol{\kappa}_A^{i_x} \\ \boldsymbol{\kappa}_B^{i_x} \end{bmatrix} = e^{-ik_L^{i_x+}S} \begin{bmatrix} \boldsymbol{\kappa}_A^{i_x} \\ \boldsymbol{\kappa}_B^{i_x} \end{bmatrix}, \tag{16a}$$

$$\boldsymbol{\kappa}_A^{i_x} = \begin{bmatrix} \kappa_1^{i_x} \\ \kappa_2^{i_x} \\ \kappa_3^{i_x} \\ \kappa_4^{i_x} \\ \kappa_5^{i_x} \\ \kappa_6^{i_x} \end{bmatrix}, \quad \boldsymbol{\kappa}_B^{i_x} = \begin{bmatrix} \kappa_7^{i_x} \\ \kappa_8^{i_x} \\ \kappa_9^{i_x} \\ \kappa_{10}^{i_x} \\ \kappa_{11}^{i_x} \\ \kappa_{12}^{i_x} \end{bmatrix}, \tag{16b}$$

where I is the identity matrix. Similarly, we can obtain the characteristic equations at the right lead.

III. FORMULATIONS OF THE RETARDED GREEN'S FUNCTIONS

To evaluate the waves excited from the left and right leads, we make use of the retarded Green's functions defined from Eq. (5) as

$$\begin{bmatrix} G_L & G_{LD} & 0 \\ G_{DL} & G_D & G_{DR} \\ 0 & G_{RD} & G_R \end{bmatrix} = \begin{bmatrix} (E+i\eta)I - H_L & -\tau_{LD} & 0 \\ -{}^t\tau_{LD} & (E+i\eta)I - H_D & -\tau_{DR} \\ 0 & -{}^t\tau_{DR} & (E+i\eta)I - H_R \end{bmatrix}^{-1}, \tag{17}$$

where G_D, G_L, and G_R are the retarded Green's functions in the CNT, the left and right leads, respectively, G_{LD}, G_{DL}, G_{DR}, and G_{RD} are the retarded Green's functions at the boundaries of the CNT and the leads, and η is the imaginary part of the energy, which is a positive infinite decimal. From Eq. (17), eliminating G_L, G_R, G_{LD}, G_{DL}, G_{DR}, and G_{RD}, we obtain

$$G_D = \left[(E+i\eta)I - H_D - \Sigma_L - \Sigma_R\right]^{-1}, \tag{18}$$

where

$$\Sigma_L = {}^t\tau_{LD} g_L \tau_{LD}, \tag{19}$$

$$g_L = \left[(E+i\eta)I - H_L\right]^{-1}. \tag{20}$$

Σ_L is referred to as the "self-energy," which represents the influence of the left lead to the CNT. Now, we let g_L be

$$g_L = \begin{bmatrix} g_{-N_L,-N_L} & g_{-N_L,-N_L+1} & \cdots & g_{-N_L,-1} \\ g_{-N_L+1,-N_L} & g_{-N_L+1,-N_L+1} & \cdots & g_{-N_L+1,-1} \\ \vdots & & \ddots & \vdots \\ g_{-1,-N_L} & g_{-1,-N_L+1} & \cdots & g_{-1,-1} \end{bmatrix}, \tag{21}$$

$$g_{j,j'} = \begin{bmatrix} g_{j,1;j',1} & g_{j,1;j',2} & \cdots & g_{j,1;j',12} \\ g_{j,2;j',1} & g_{j,2;j',2} & \cdots & g_{j,2;j',12} \\ \vdots & & \ddots & \vdots \\ g_{j,12;j',1} & g_{j,12;j',2} & \cdots & g_{j,12;j',12} \end{bmatrix}, \quad j,j' = -N_L, -N_L+1, \cdots, -1. \tag{22}$$

Then, from Eqs. (7), (19), (21), and (22), we obtain

$$\sum_L = \left[\begin{array}{c|c} {}^tVg_{-1,-1}V & 0 \\ \hline 0 & 0 \end{array}\right]. \tag{23}$$

For the zigzag CNT, ${}^tVg_{-1,-1}V$ is expressed as

$${}^tVg_{-1,-1}V = \left[\begin{array}{cccccc|c} \gamma_1^2 g^L_{7,7} & 0 & \gamma_1^2 g^L_{7,9} & 0 & \gamma_1^2 g^L_{7,11} & 0 & \\ 0 & 0 & 0 & 0 & 0 & 0 & \\ \gamma_1^2 g^L_{7,7} & 0 & \gamma_1^2 g^L_{7,9} & 0 & \gamma_1^2 g^L_{7,11} & 0 & 0 \\ 0 & 0 & 0 & 0 & 0 & 0 & \\ \gamma_1^2 g^L_{7,7} & 0 & \gamma_1^2 g^L_{7,9} & 0 & \gamma_1^2 g^L_{7,11} & 0 & \\ 0 & 0 & 0 & 0 & 0 & 0 & \\ \hline \multicolumn{6}{c|}{0} & 0 \end{array}\right]. \tag{24}$$

Equation (24) means that Σ_L can be expressed in terms of only nine equilibrium Green's functions $g^L_{k,k'}(k,k'=7,9,11)$ for $n=3$. We can obtain Σ_R in a similar manner. For armchair and chiral CNTs, we can obtain similar equations by following the above derivation.

Two equilibrium Green's functions g_L and g_R are evaluated as the limits when N_R and N_L go to infinity. For the one-dimensional case, the equilibrium Green's function can simply be calculated in semi-infinite electrodes at both ends of the device.[7] For CNT models, on the other hand, it is difficult to express the equilibrium Green's function in a simple form. Therefore, we use the following procedure.

(1) Transform the wave functions on the tight-binding (TB) basis into the corresponding wave functions on the PW basis.
(2) Find solutions to the PWs in semi-infinite electrodes at both ends of the device, at which the periodic nature of electrodes in thermal equilibrium can be exploited.
(3) Inverse transform the wave functions on the PW basis into those on the TB basis.

Then, from Eqs. (5), (12), (13a), and (14a), the equation for the plane waves propagating to one direction with real wave vectors should satisfy the following equation:

$$E\boldsymbol{\psi}_0 = {}^tVU_L P_L^+ U_L^{-1}\boldsymbol{\psi}_0 + H_0\boldsymbol{\psi}_0 + V\boldsymbol{\psi}_1. \tag{25}$$

In Eq. (25), P_L^+ is the following matrix comprised of the factors $e_L^{i_x+} \equiv \exp(-ik_L^{i_x+}S)(i_x=1,2,\ldots,n_l)$:

$$P_L^+ = \left[\begin{array}{ccc|c} e_L^{1+} & & 0 & \\ & \ddots & & 0 \\ 0 & & e_L^{n_l+} & \\ \hline \multicolumn{3}{c|}{0} & 0 \end{array}\right], \tag{26}$$

where n_l is the number of plane waves propagating in one direction along with the real wave vectors, and U_L is the following unitary matrix that is comprised of the characteristic vectors of the characteristic equation, Eq. (16a):

$$U_L \equiv \left[\begin{array}{cccc|cccc} \kappa_1^1 & \kappa_1^2 & \cdots & \kappa_1^6 & \lambda_1^1 & \lambda_1^2 & \cdots & \lambda_1^6 \\ \kappa_2^1 & \kappa_2^2 & & \kappa_2^6 & \lambda_2^1 & \lambda_2^2 & & \lambda_2^6 \\ \vdots & & \ddots & \vdots & \vdots & & \ddots & \vdots \\ \kappa_{12}^1 & \kappa_{12}^2 & \cdots & \kappa_{12}^6 & \lambda_{12}^1 & \lambda_{12}^2 & \cdots & \lambda_{12}^6 \end{array}\right]. \tag{27}$$

Using Eq. (25), the equilibrium Green's function $g_{-1,-1}$ is expressed as

$$g_{-1,-1} = \{(E+i\eta)I - H_0 - {}^tVU_L P_L^+ U_L^{-1}\}^{-1}, \tag{28}$$

and we can then obtain the equilibrium Green's function at the left end lead: $g^L_{k,k'} \equiv g_{-1,k;-1,k'}$. Similarly, we can obtain the equilibrium Green's function at the right lead: $g^R_{k,k'} \equiv g_{N+1,k;N+1,k'}$.

IV. CHARGE DENSITY AND CURRENT IN CNTs

The left and right spectral functions A_L and A_R can be defined as

$$A_L = G_D \Gamma_L G_D{}^\dagger, \tag{29a}$$

$$A_R = G_D \Gamma_R G_D{}^{\dagger}, \tag{29b}$$

where $A_L/2\pi$ and $A_R/2\pi$ correspond to the local density of states.[7] We use G_D in Eq. (18) to obtain these spectral functions. Γ_L and Γ_R in Eq. (29) are expressed using Eq. (23) as

$$\Gamma_L = i[\Sigma_L - \Sigma_L^{\dagger}], \tag{30a}$$

$$\Gamma_R = i[\Sigma_R - \Sigma_R^{\dagger}]. \tag{30b}$$

We can express the transmission coefficient T as

$$T = \Gamma_L G_D \Gamma_R G_D{}^{\dagger}, \tag{31}$$

which is typically interpreted as the probability that an electron will transfer from the left contact to the right contact.[7]

Next, we calculate the charge density as incoming carriers from the left and the right leads. Since the left lead excites electrons with $E=E_0 \sim \infty$, we can obtain the electron density entering from the left lead by integrating the product of $\{A_L\}_{j,k;j,k}$ and the Fermi-Dirac function within the energy range. On the other hand, since the right lead excites electrons with $E=E_N \sim \infty$, we fill the right spectral function $\{A_R\}_{j,k;j,k}$ according to the right Fermi-Dirac function from E_N to ∞ in the right lead. Now, electronic density $n_{j,k}$ can be expressed as

$$n_{j,k} = \int_{E_0}^{\infty} \frac{dE}{2\pi} \{A_L\}_{j,k;j,k} f(E-\mu_L) + \int_{E_N}^{\infty} \frac{dE}{2\pi} \{A_R\}_{j,k;j,k} f(E-\mu_R), \tag{32}$$

which is interpreted as the sum of the two incoming waves, where f is the Fermi-Dirac distribution function expressed as

$$f(E-\mu) = \frac{1}{1+\exp[(E-\mu)/k_B T]}, \tag{33}$$

where T is the temperature, k_B is the Boltzmann factor, and μ_L and μ_R are the microseconds shown below in the left and right leads, respectively.

$$\mu_L = E_0 + E_F, \tag{34a}$$

$$\mu_R = E_N + E_F, \tag{34b}$$

where E_F is the position of the Fermi level. $\{A_L\}_{j,k;j,k}$ and $\{A_R\}_{j,k;j,k}$ in Eq. (32) represent diagonal components of the left and right local density of states, respectively. In the same way, hole density $p_{j,k}$ can be expressed as

$$p_{j,k} = \int_{-\infty}^{E_0} \frac{dE}{2\pi} \{A_L\}_{j,k;j,k} f(\mu_L - E) + \int_{-\infty}^{E_N} \frac{dE}{2\pi} \{A_R\}_{j,k;j,k} f(\mu_R - E). \tag{35}$$

On the other hand, we can obtain the current I as

$$I = \frac{2q}{h} \int_{-\infty}^{\infty} dE \sum_{k=1}^{4n} \sum_{j=0}^{N} \{T\}_{j,k;j,k} \left[f(E-\mu_L) - f(E-\mu_R) \right], \tag{36}$$

where we integrate the product of $\{T\}_{j,k;j,k}$ and the Fermi-Dirac function. Since we have assumed that the electrostatic potential U_j in the jth CUC is constant, as shown in Fig. 1, we can obtain

$$E_j = U_j + \epsilon_0, \tag{37}$$

where ϵ_0 is the on-site energy of the carbon atom: $\epsilon_0 = -2.18$ eV.[13]

A. Transport characteristics in *zigzag* CNTs

Figures 2(a) through 2(c) show the electron density distribution, the hole density distribution, and the *I-V* characteristics, respectively, for a metallic and intrinsic CNT with (6, 0) chirality. The distributions n_j and p_j are obtained from

$$n_j \equiv \frac{1}{2\pi c_0 r_{\mathrm{CNT}} S} \sum_{k=1}^{4n} n_{j,k}, \tag{38a}$$

$$p_j \equiv \frac{1}{2\pi c_0 r_{\mathrm{CNT}} S} \sum_{k=1}^{4n} p_{j,k}, \tag{38b}$$

where r_{CNT} is the radius of the CNT, S is $\sqrt{3}a_0$ for the zigzag CNT, a_0 and c_0 are the lattice constants of the hexagonal graphite,[14,15] $a_0 = 0.246\,12$ nm,[16] and $c_0 = 0.6707$ nm.[17] We chose γ_3 to 10^{-3} times γ_1 for the zigzag CNT, which was adjusted in order to show the almost same transport characteristics as those for $\gamma_3 = 0$. Figures 2(a) and 2(b) indicate that no significant difference exists between n_j and p_j, the distributions of which are uniform. Because Figs. 2(a) and 2(b) show that charge neutrality throughout the CNT is satisfied, the assumption of the linearly varying potential is found to be valid for our calculation. The *I-V* characteristics of Fig. 2(c) agree sufficiently with those obtained by the transfer-matrix method.[6]

The complex *E-k* dispersion curves are shown in Fig. 3, in which the thick lines correspond to the dispersion curves for the Bloch waves and the thin lines correspond to those for the evanescent modes or decaying waves in the electrodes. In Fig. 3, the labels b1, b2,…, b5, a1, a2, a3 indicate the dispersion curves with real wave vectors (Bloch waves). The two "↕'s" show the energy ranges of carriers excited at the left and right leads when the applied bias V_0 is 1.5 V. The length of each arrow corresponds to each applied bias voltage, where the transport or transition b1→b1, b2→b1,…, b5→b1, or b1→a1 occurs.

Figures 4(a) and 4(b) show the *I-V* and *G-V* characteristics of the (16, 0) CNT, respectively, where the position of the Fermi level is assumed to be $E_F = -0.26$ eV and G is the differential conductance defined by $\partial I/\partial V$. The *G-V* characteristics are classified into the following three regions with respect to the bias voltage V_0.

(I) The transition b1→b1 contributes primarily to the current I, which increases as V_0 increases.

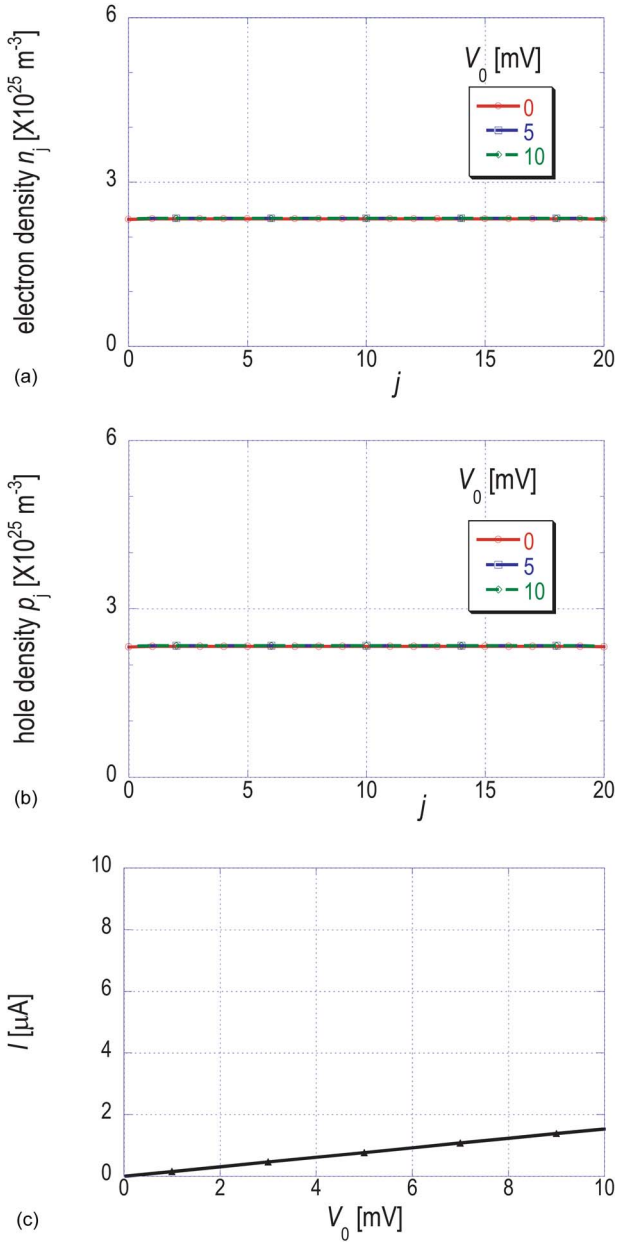

FIG. 2. (Color online) Characteristics of the (6, 0) CNT. (a) electron density distribution, (b) hole density distribution, and (c) *I-V* characteristics. E_F =0 eV, $\gamma_3=10^{-3}\gamma_1$, $N=20$, and $T=300$ K.

(II) The transition b1→b1 dominates the current I, which is approximately constant. In a part of this region, G is found to be negative because the transmission coefficient decreases as the difference in the group velocities between the incoming and outgoing waves becomes large with the increase of the applied bias (see Figs. 3 and 4).

(III) In addition to the transition b1→b1, the transfer b1→a1 begins to contribute to I. The conductance G in this region is found to decrease as the length N of the CNT becomes longer because the electronic wave of the transition b1→a1 is an evanescent mode and attenuates drastically as it propagates in the CNT.

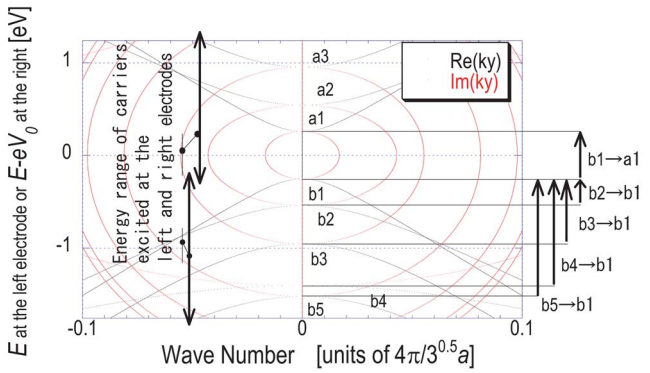

FIG. 3. (Color online) Dispersion curves at the left and right leads of the (16, 0) CNT. The labels "↕" indicate the energy range of the electrons or holes excited in the leads when $V_0=1.50$ V and $E_F=-0.26$ eV. The labels b1, b2,… b5, a1, a2, a3 indicate the dispersion curves with real wave vectors (Bloch waves).

Figures 5(a)–5(c) show the *GV/I-V* characteristics of a (16, 0) CNT. The solid, dash-dotted, and dashed lines correspond to the *GV/I-V* characteristics with $N=5$, 10, and 20, respectively. The label "↑" or "↓" in Figs. 5(a)–5(c) indicates the onsets of the transitions b1→b1, b2→b1, b3→b1, b4→b1, and b5→b1, respectively.

GV/I takes maximum values at $V_0=0$ and 1.27 V, independent of the length N, as shown in Figs. 5(a) and 5(b). *GV/I* takes a maximum value at $V_0=0.68$ V when $N=20$ in Fig. 5(c). When $N=5$ and 10, the maximum value of *GV/I* at V_0 is 0.6 V, which obscures that occurring at $V_0=0.68$ V.

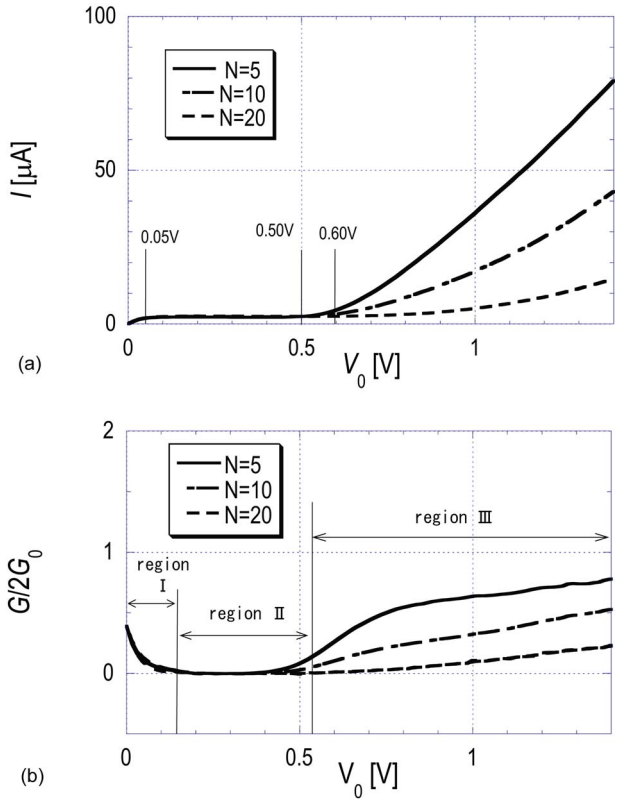

FIG. 4. (Color online) Characteristics of the (16, 0) CNT. (a) *I-V* characteristics and (b) *G-V* characteristics. $N=5$ (solid lines), 10 (dash-dotted lines), 20 (dashed lines), $E_F=-0.26$ eV, and $T=300$ K.

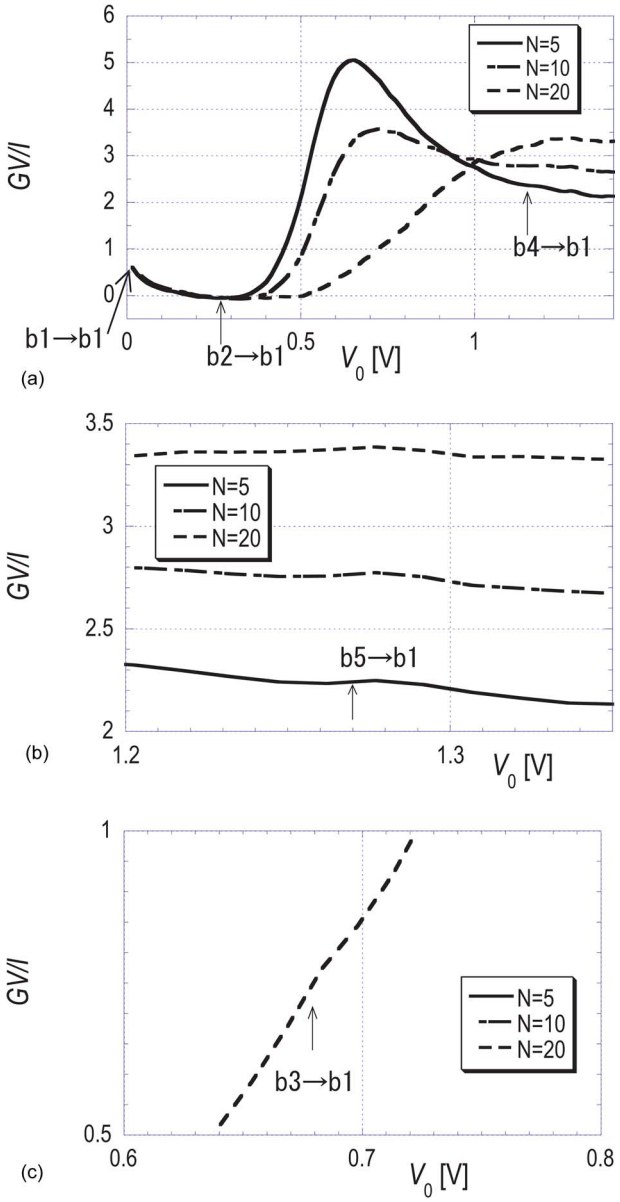

FIG. 5. (Color online) GV/I-V characteristics of the (16, 0) CNT. (a) $V_0=0-1.4$ V, (b) $V_0=1.2-1.35$ V, and (c) $V_0=0.6-0.8$ V. $N=5$ (solid lines), 10 (dash-dotted lines), 20 (dashed lines), $E_F=-0.26$ eV, and $T=300$ K.

However, when $N=20$, the maximum of 0.6 V almost vanishes. This maximum appears to be contributed to the current due to the transition b1→a1, because transition b1→a1 is an attenuating electronic wave. The characteristic applied voltages of 0, 0.68, and 1.27 V correspond to the voltages of the onsets of the transitions b1→b1, b3→b1, and b5→b1, respectively. On the other hand, GV/I does not show a maximum at the start of the transitions b2→b1 or b4→b1 because whether GV/I takes a maximum at the opening of the transition bi→b1 ($i=1,2,3,4,5$) depends on the magnitude of the difference between the group velocities of bi and b1. Because the group velocities are proportional to the slopes of the dispersion curves (Fig. 3), and because those of b3 and b5 are comparable to that of b1 in Fig. 3, the transitions b1→b1, b3→b1, and b5→b1 contribute considerably to the current. In contrast, the transitions b2→b1 and b4→b1 contribute less to the current, for the same reason described above for the transitions b3→b1 and b5→b1.

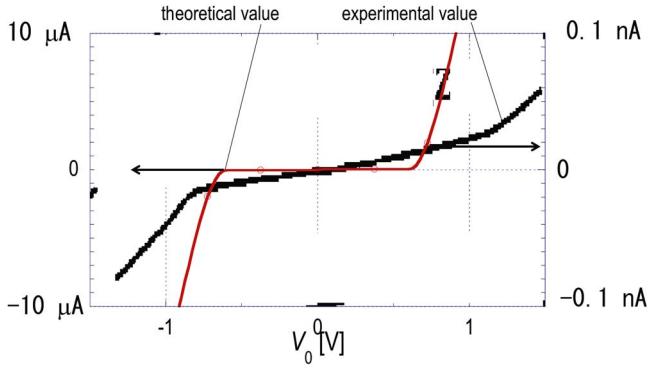

FIG. 6. (Color online) I-V characteristics of the (14, 0) CNT. Theoretical value (gray solid line) and experimental data (black solid line). $E_F=-0.2$ eV, $N=5$, and $T=300$ K.

It has been reported that the GV/I characteristics take maximum values at $V_0=0.7$ and 1.2 V in the experiment applied to the zigzag CNT.[11] These two voltages can be ascribed to the transitions b1→b1 and b3→b1, respectively, because these two values are comparable to those of the onsets of the transitions. This agreement indicates that the application of our simulation to the analysis of the transport in CNTs is appropriate.

Figure 6 shows the I-V characteristics of a (14, 0) CNT. The black solid line indicates the experimental characteristics reported in Ref. 11 and the gray solid line indicates the theoretical values of the present study. The experimental current I is of nanoampere dimension, which is much smaller than the theoretical value, which is of microampere dimension. The difference between the experimental and theoretical values is due to possible existence of contact resistances between the CNT and the leads. The I-V characteristics have two bends in the positive and negative bias regions, respectively. In the negative bias region, both the experimental and theoretical values are −0.8 V. In the positive V_0 area, the experimental and theoretical values are +1.2 and +0.8 V, respectively. The difference between these values may be ascribed to the voltage rectifying characteristics of the contact, such as those of the Schottky junction between the CNT and the leads.

B. Transport characteristics of *armchair* CNTs

We have evaluated the I-V and G-V characteristics of the (18, 18) CNT, as shown in Figs. 7(a) and 7(b), respectively, where $E_F=-0.4$ eV. We chose γ_3 to 10^{-4} times γ_1 for the armchair CNT, which was adjusted in the same manner as the zigzag CNT. In this case, the I-V and G-V characteristics consist of the following three regions.

(I) I increases with the increase of the bias voltage V_0 due to the transitions b1→b1 and b2→b2, as shown in Fig. 8. Since the differential conductance G consists of the components from the transition b1→b1 and that contributed by the transition b2→b2, G exceeds $2G_0$ in this region, where G_0 is the conductance quantum.

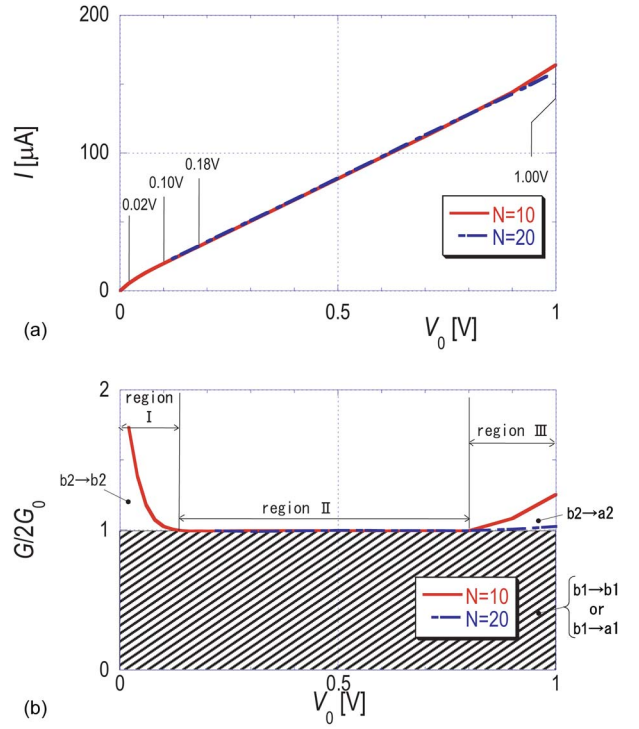

FIG. 7. (Color online) Characteristics of the (18, 18) CNT. (a) *I-V* characteristics and (b) *G-V* characteristics. $E_F=-0.4$ eV, $T=300$ K, and $\gamma_3=10^{-4}\gamma_1$.

(II) The contribution from the transition b2→b2 diminishes, and the transition b1→b1 dominates the current, which results in the constant conductance $2G_0$.

(III) In addition to the transitions b1→b1 and b2→b2, since the transition b2→a2 starts to contribute to the current, the current increases in this region. The conductance G, however, approaches $2G_0$ as the length of the CNT N increases because the electronic wave of the transition b2→a2 is the evanescent mode, which attenuates in the CNT.

We have not compared the theoretical characteristics of the (18, 18) CNT obtained in the present study with the experimental characteristics because, thus far, there has been no corresponding report. The GFM has been successfully applied to the analysis of quantum transport in the zigzag and armchair CNTs and is applicable to the analysis of chiral-type CNTs.

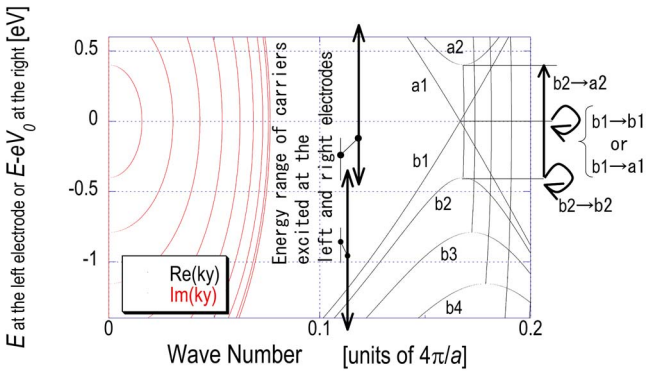

FIG. 8. (Color online) Dispersion curves at the left and right leads of the (18, 18) CNT. The labels "↕" indicate the energy range of electrons and holes excited in the leads as $V_0=1.0$ V and $E_F=-0.4$ eV. Labels b1, b2, b3, b4, a1, and a2 indicate the dispersion curves with real wave vectors.

V. CONCLUSION

We have formulated and applied Green's-function method to the analysis of quantum transport in the CNTs. The simulation revealed that the assumption of a linearly varying potential distribution is valid for metallic and intrinsic CNTs because the electron and hole densities satisfy the charge neutrality condition. We evaluated the *I-V* characteristics of the semiconductive (16, 0) and metallic (18, 18) CNTs. Based on these characteristics, we can control the differential conductance G from a negative value to a value several times the conductance quanta by means of chirality, position of the Fermi level, and bias voltage. More significantly, when the group velocity of a mode b_i with a real wave vector is comparable to that of another mode b_j, GV/I takes a maximum at the specific bias voltage that corresponds to the transition between these modes.

Since the GFM formulation described herein is applicable to CNTs with arbitral chirality and defects of carbon atoms or other impurity atoms, we can evaluate not only metallic CNTs but also semiconductive and insulating CNTs as well. Because this method can evaluate electron and hole densities as well as current in CNTs, we can simultaneously solve the transport and Poisson equations. This GFM formulation can be further extended to

(1) evaluate alternating current and
(2) evaluate interactions between electronic wave and electromagnetic fields

in CNTs.

In the future, we plan to develop the above-mentioned method for analyzing CNTs used as nanoelectrodes in ferrite devices, which act as a filter in the terahertz domain.[6] The GFM method described herein may be applicable to a wide variety of device designs and applications.

[1] R. Tamura and M. Tsukada, Phys. Rev. B **55**, 4991 (1997).
[2] T. Ando, T Nakanishi, and M. Igami, J. Phys. Soc. Jpn. **68**, 3994 (1999).
[3] M. P. Anantram, Phys. Rev. B **62**, R4837 (2000).
[4] F. Triozon, S. Roche, A. Rubio, and D. Mayou, Phys. Rev. B **69**, 121410 (2004).
[5] S. Latil, S. Roche, D. Mayou, and J. C. Charlier, Phys. Rev. Lett. **92**, 256805 (2004).
[6] T. Umegaki, M. Ogawa, Y. Makino, and T. Miyoshi, J. Appl. Phys. **96**, 6669 (2004).
[7] S. Datta, Superlattices Microstruct. **28**, 253 (2000).
[8] L. F. Chibotaru, S. Compernolle, and A. Ceulemans, Phys. Rev. B **68**, 125412 (2003).
[9] M. P. Anantram, S. Datta, and Y. Xue, Phys. Rev. B **61**, 14219 (2000).
[10] M. Ogawa, T. Sugano, and T. Miyoshi, Solid-State Electron. **44**, 1939 (2000).
[11] J. W. G. Wildoer, L. C. Venema, A. G. Rinzler, R. E. Smalley, and C. Dekker, Nature (London) **391**, 59 (1998).
[12] X. Blase, L. X. Benedict, E. L. Shirley, and S. G. Louie, Phys. Rev. Lett. **72**, 1878 (1994).
[13] D. L. Greenaway and G. Harbeke, Phys. Rev. **178**, 1340 (1969).
[14] J. D. Bernal, Proc. R. Soc. London **A106**, 749 (1924).
[15] O. Hassel and H. Mark, Z. Phys. **25**, 317 (1924).
[16] H. Lipson and A. R. Stokes, Proc. R. Soc. London **A181**, 101 (1942).
[17] J. B. Nelson and D. P. Riley, Proc. Phys. Soc. London **57**, 477 (1945).